Richter, C. (Ed.)
Proceedings of the Ocean Drilling Program, Scientific Results Volume 181

3. Data Report: Miocene to Pleistocene Sedimentation Pattern on the Chatham Rise, New Zealand[1]

Amelie Winkler[2,3] and Wolf-Christian Dullo[3]

ABSTRACT

Site 1123 is located on the northeastern flank of the Chatham Rise. Sedimentological and clay mineralogical analyses indicate a very fine grained carbonate-rich sediment. Smectite and illite are the main constituents of the clay mineral assemblage. High smectite values in the Eocene decrease in younger sediment sequences. Illite and chlorite concentrations increase in younger sediments with significant steps at 13.5, 9, and 6.4 Ma. The kaolinite content is near the detection limit and not significant. We observed only small fluctuations of the clay mineral composition, which indicates a uniform sedimentation process, probably driven by long-term processes. Good correspondence is shown between increasing illite and chlorite values and the tectonic uplift history of the Southern Alps.

INTRODUCTION

The Southwest Pacific east of New Zealand is a key region of the global thermohaline conveyor hypothesis as suggested by Broecker et al. (1990) and Schmitz (1995). The opening of the Tasman gateway and the Drake Passage between 32 and 20 Ma (Kennett et al., 1972, Boltovskoy, 1980) allowed for the evolution of the Antarctic Circumpolar Current–Deep Western Boundary Current system (ACC-DWBC) (Molnar et al., 1975, Lawver et al., 1992). The DWBC transports ~20 × 10^6 m^3/s of water into the Pacific, which composes ~40% of the total input of deep water to the world's oceans (Warren, 1973, 1981). This deep wa-

[1] Winkler, A., and Dullo, W.-C., 2002. Data report: Miocene to Pleistocene sedimentation pattern on the Chatham Rise, New Zealand. *In* Richter, C. (Ed.), *Proc. ODP, Sci. Results,* 181, 1–21 [Online]. Available from World Wide Web: <http://www-odp.tamu.edu/publications/181_SR/VOLUME/CHAPTERS/206.PDF>. [Cited YYYY-MM-DD]
[2] Bundesanstalt für Geowissenschaften und Rohstoffe, Stilleweg 2, D-30655 Hannover, Germany.
a.winkler@bgr.de
[3] GEOMAR Research Center for Marine Geosciences, Wischhofstrasse 1-3, Gebäude 4, D-24148 Kiel, Germany.

Initial receipt: 11 April 2001
Acceptance: 2 October 2001
Web publication: 14 March 2002
Ms 181SR-206

ter is produced in the Weddell and Ross Seas and mixed with North Atlantic Deep Water (NADW) in the Atlantic Sector of the Southern Ocean.

In the pathway of the DWBC along the New Zealand margin, some sediments drifts were discovered through seismic analyses (Fulthorpe and Carter, 1991; Carter and McCave, 1994; Carter et al., 1996). At the eastern flank of the Chatham Rise, a drift was created due to the deceleration of the DWBC after passing the Valerie Passage, a 250-km-wide gap between the Chatham Rise and the Louisville Seamount (Warren, 1973).

Various sediment sources contribute to the sedimentation process. In addition to the biopelagic sedimentation, material from other distant sources is transported by the DWBC. Evidence for long distance transport is provided by the presence of subantarctic diatoms in the drift at 40°S (Carter and Mitchell, 1987). The airfall of rhyolitic and andesitic tephra from the arc volcanism in New Zealand since the Miocene (e.g., Nelson et al., 1986; Shane and Froggatt, 1991; Carter et al., 1995; Shane et al., 1995) represents another sediment source. Further sediment input is fed to the DWBC by the uplift and erosion of the Southern Alps of New Zealand. Beginning ~24 Ma, the material from the Southern Alps was eroded (Vella, 1962; Norris et al., 1978) and transported from the eastern South Island to the Solander Channel, Bounty Trough, and Hikurangi Channel system.

The sedimentation pattern and the path of redistribution along the eastern continental margin of New Zealand will shed light on the climatic development, the tectonic history, and the evolution of the DWBC.

The focus of this study is the middle to late Miocene time interval, during which significant cooling of Antarctica has been described (Flower and Kennett, 1995).

SEDIMENT COMPOSITION OF SITE 1123

Site 1123 is located on the northeastern flank of the Chatham Rise in a water depth of 3290 m. It was drilled in a sediment drift that was built as a result of the decelerating DWBC after passing the Valerie Passage.

Three holes were cored at Site 1123. Hole 1123A reached a maximum depth of 158.1 meters below seafloor (mbsf), Hole 1123B penetrated to 489 mbsf, and Hole 1123C penetrated to 632.80 mbsf. The sediment is comprised of clayey nannofossil ooze with an increasing degree of lithification with depth (Carter, McCave, Richter, Carter, et al., 1999). Site 1123 is subdivided into four lithologic units. Unit I, which is Pleistocene to late Miocene in age, extends from the seafloor to 256.59 mbsf and consists of clayey nannofossil ooze (Subunit IA) and chalk (Subunit IB). Tephra layers are very abundant in Subunit IA and are also present in Subunit IB. Unit II (257 to 450.8 mbsf) spans the late Miocene to middle Miocene. This uniform sedimentary sequence is composed of clayey nannofossil chalk containing nine tephra layers. The underlying Unit III ranges from middle Miocene to early Miocene in age (450.8 to 587.2 mbsf). The base of Unit III is set below the mid-Oligocene Marshall Paraconformity (Fulthorpe et al., 1996). The abundance of terrigenous clay increases in Unit III, and the sediment composition changes from clayey nannofossil chalk to nannofossil mudstone. Within Unit III (542.9 to 550.5 mbsf) a debris flow interrupts the continuous sedi-

mentary sequence. Unit IV reaches 632.8 mbsf and consists of micritic limestone.

METHODS

Organic and Inorganic Carbon Analyses

The bulk samples of Hole 1123B and Hole 1123C were split into subsamples. One subsample was analyzed for carbonate and total organic carbon (TOC) content with a Leco CS-125 analyzer. Double measurements were performed on total carbon (TC) after decarbonization of the sample on TOC. The content of calcium carbonate was calculated by multiplying the difference between TC and TOC by a factor of 8.333.

Clay Mineral Analyses

After separating the fine fraction through wet sieving, it was treated with 10% H_2O_2 to remove organic carbon. After washing the sample, calcium carbonate was dissolved with 6% acetic acid. Repeated washing and centrifugation then cleared the sample of acid. Sodium polyphosphate of 0.05% concentration was added for dispersion of the fine fraction. After this pretreatment, an aliquot of the <2-µm fraction was separated by the settling method according to Stoke's law.

Oriented samples were produced using the filter transfer method (Moore and Reynolds, 1997). Depending on the concentration of the suspension, an appropriate quantity was sucked through a 0.2-µm cellulose nitrate filter to yield an "infinite" sample thickness corresponding to 14 mg/cm². The sample cake was dried overnight at 50°C and transferred to an aluminum slide. Analyses were performed using a Philips X-ray diffractometer 1830 with CoK_α radiation (40 kV; 35 mA), automatic divergence slit, graphite monochromator, and automatic sample holder. XRD scans with a step width of 0.01°2θ/s were carried out on untreated samples and after glycolation (12 hr at 60°C) in a range of 2°–40°2θ.

Peak areas of base reflections were calculated using MacDiff software v. 3.1 (R. Petschick) (**http://servermac.geologie.uni-frankfurt.de/Staff/Homepages/Petschick/RainerE.html**) after manual correction of the baseline for

1. Smectite (including randomly interstratified illite/smectite mixed layers and smectite/chlorite mixed layer minerals) at 17.2–16.7 Å after graphical removal of the chlorite peak at 14 Å,
2. Illite (including regular illite-smectite mixed layers) at 10.1 Å, and
3. Chlorite and kaolinite at 7.1 Å.

The peak areas of the coincident peaks of chlorite (002) and kaolinite (001) were subdivided using the intensity ratio of chlorite (004) at 3.54 Å and kaolinite (002) at 3.58 Å (Biscaye, 1964). The terms smectite, illite, chlorite, and kaolinite are used here as general expressions for the corresponding mineral groups. Mixed layer minerals that were indicated by broadening of peaks and only present in trace amounts were not calculated.

The relative percentages were calculated using the empirically estimated factors by Biscaye (1965). The precision of repeated measure-

ments has a standard deviation <3.5% (Winkler et al., 2001). The S/(I+C+S) ratio is based on the uncorrected peak areas.

Age-Depth Model

The age-depth model is mainly based on magnetostratigraphy, which is compared to the geomagnetic polarity timescale of Cande and Kent (1995) and Berggren et al. (1995) according to the shipboard age-depth model (Carter, McCave, Richter, Carter, et al., 1999). Two biostratigraphic datums were added to the age-depth model at 21.6 Ma at 596.7 meters composite depth (mcd) and 30 Ma at 597 mcd. A significant hiatus of at least 9 m.y. is present between 21 and 30 Ma. The debris flow (Subunit IIIB) occurs from the interval from 552.46 to 560.06 mcd and was excluded by the calculation of the linear age and accumulation rates.

Bulk Accumulation Rates

The bulk accumulation rates (Bulk AR) were calculated by using the shipboard gamma ray attenuation (GRA) density data with the following formula:

$$\text{Bulk AR} = \text{LSR} \times \text{GRA},$$

where

Bulk AR = accumulation rate of the bulk sediment (g/cm²/m.y.),
LSR = linear sedimentation rate (cm/m.y.), and
GRA = gamma ray attenuation bulk density (g/cm³).

DATA DESCRIPTION

The sediment of Site 1123 is very fine grained consisting of a <63-µm fraction to >97 wt% on average. A significant occurrence of coarser particles is present in Oligocene sediments comprising 2 wt% of the >63-µm fraction. A similar coarse fraction occurs at ~16 Ma with several events containing 3 to 4 wt% of the >63-µm fraction. At 4.5 Ma, a single event of 5 wt% coarse-fraction input occurs. In the Pleistocene, the content of the coarse fraction (<63 µm) rises to 10 wt% (Fig. **F1;** Table **T1**).

Sedimentation at the northeastern flank of the Chatham Rise shows high carbonate content with an average of 50 wt% (Fig. **F1**). The very high carbonate content in Eocene sediments of 70–80 wt% decreases in early to middle Miocene time with minimum values of 20 wt% $CaCO_3$. An increasing trend begins at 14.4 Ma with values of 60–70 wt%. This level of high carbonate content is relatively constant until 9 Ma. A period with lower carbonate content and stronger fluctuations around 50 wt% follows. Between 3.5 and 1.5 Ma, a significant decrease of $CaCO_3$ concentration occurs.

The overall TOC content averages <0.5 wt% (Fig. **F1**). Several single peaks of a higher TOC content (0.5 to 1 wt%) occur at 17.7, 9.7, 5.6, 4.4 Ma, between 2 and 1.5 Ma, and at 0.7 Ma. In general, the TOC content increases slightly in younger sediments but remains on average below 0.5%.

F1. Bulk AR, coarse fraction content, $CaCO_3$ content, and TOC; Site 1123, p. 9

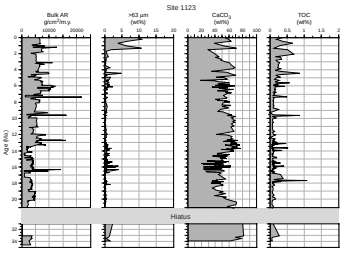

T1. Bulk AR, >63 µm, $CaCO_3$, and TOC, p. 11.

The high resolution of the age-depth model at Site 1123 allows the calculation of a detailed record of bulk accumulation rates (bulk AR; Fig. F1). This shows single events of maximum accumulation at 16.5 to 16.3 Ma and at 12.7, 9.6, and 7.3 Ma. Sediments older than 13.5 Ma display a bulk AR of 3000 to 4000 g/cm²/m.y. In this older sediment sequence the bulk AR exceeds values of ~5000 g/cm²/m.y. only between 20 and 19 Ma. Beginning at ~13.5 Ma, the bulk AR is marked by values of ~6000 g/cm²/m.y., however the bulk accumulation rate reaches values below 5000 g/cm²/m.y. several times (e.g., 11.9 to 11.1 Ma, 9.9 to 9.6 Ma, at 9.5 Ma, 9.2 to 9.1 Ma, and 7.3 to 7.1 Ma).

The clay mineral distribution is dominated by smectite and illite and shows an inverse correlation throughout the sedimentary sequence (Fig. F2; Table T2). Kaolinite and chlorite play a subordinate role in the total clay mineral assemblages. In general, the chlorite percentages are lower but mimic the illite content. Eocene sediments contain 80% smectite, whereas illite is low (10% to 15%). In the lower Miocene (20 to 18.5 Ma), smectite values are still high, with an average of 60%. A significant decrease to 45% smectite occurs at 18 Ma. At the same time illite increases slightly to 33% and the chlorite concentration is 15%, compared to the low chlorite content of <5% in the Eocene, and a value of nearly 10% in the early Miocene.

A significant shift to lower smectite content and higher illite and chlorite values appears for the first time at 13.5 Ma. Smectite decreases to a level of nearly 50%, whereas illite increases to 38% and chlorite to ~15%. The smectite concentration remains almost constant until 10 Ma and then rapidly decreases to about 30% at 9 Ma. Illite and chlorite increase in the same section. Starting at 9 Ma, illite shows an average value of 45% and chlorite increases to values of 25%. At 6 Ma, smectite decreases below 20%. With maximum values of 6% in the lower Miocene, kaolinite does not contribute significantly to the clay mineral composition. In the younger sedimentary sequence, the content of kaolinite decreases to 3% on average. This is close to the analytical detection limit.

In Figure F2, column 5, the ratio of smectite to illite, plus chlorite, plus smectite is shown. Because of the very good correlation between smectite and illite and chlorite, this is a useful parameter for describing the variability of the entire clay mineral composition with a single parameter.

F2. Distribution of sediments and the ratio of S/(I+C+S) in the clay fraction, Site 1123, p. 10.

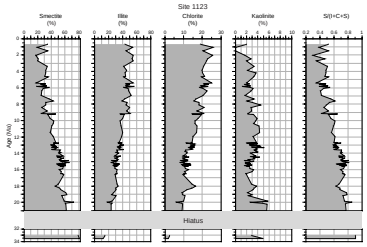

T2. Smectite, illite, kaolinite, chlorite, and S/(I+C+S) ratio, p. 20.

DISCUSSION

The high smectite content ~80% in Eocene sediments corresponds well with the findings of Robert et al. (1986) at Site 594 on the Chatham Rise. They suggest that during this time interval smectite was formed in plains and perimarine lagoons which resulted in high smectite values in Eocene sediments around New Zealand. The increased content of illite and chlorite in lower Miocene sediments at Site 1123 could be explained by enhanced sediment supply shed from the uplifting of the Southern Alps, which commenced in the late Oligocene (Vella, 1962; Norris et al., 1978).

During the transition from the early to the middle Miocene, the ratio of S/(I+C+S) decreases only slightly. The bulk AR is relatively uniform between 20 and 15 Ma, with an average of 4000 to 5000 g/cm²/m.y. In the sediments corresponding to this time interval, the calcium carbonate content is low, suggesting a more terrigenous source.

Despite the weak trend to a lower S/(I+C+S) ratio during the early middle Miocene, a significant qualitative change in the clay mineral composition is not documented before 13.5 Ma. The bulk AR shows an increase at 13.5 Ma. An increase in calcium carbonate content at 14 Ma predates the increase of the accumulation rate by 0.5 Ma. This indicates a synchronous increase of bulk AR and a fine fraction composition shift, possibly caused by a new sediment source or strengthening of the influence of one source in a suite of different sources starting at 13.5 Ma.

The increase of illite and chlorite at ~9 Ma is linked to higher terrigenous input associated with decreasing carbonate values in comparison to unaltered bulk AR.

A significant shift of clay mineral composition occurs between 7.6 and 6.4 Ma with a strong increase of chlorite related to short-term doubling of the accumulation rate from 6.5 to 6 Ma. This may indicate accelerated erosion because of increased collision of plate boundaries at ~6.4 Ma as suggested by Walcott (1998).

Short-term fluctuations of the clay mineral composition indicate very uniform sedimentation conditions. This is particularly evident during the early and middle Miocene, which is documented by a higher sample resolution. Our data suggest that the sediment composition at Site 1123 is influenced by long-term variations, such as tectonic processes at the Alpine Fault.

ACKNOWLEDGMENTS

We thank Nicole Januszczak for the constructive and helpful review. This research used samples provided by the Ocean Drilling Program (ODP). The ODP is sponsored by the U.S. National Science Foundation (NSF) and participating countries under management of Joint Oceanographic Institutions (JOI), Inc. Funding for this research was provided by the Deutsche Forschungsgemeinschaft DFG, Project Number DU 129/22-1.

REFERENCES

Berggren, W.A., Hilgen, F.J., Langereis, C.G., Kent, D.V., Obradovich, J.D., Raffi, I., Raymo, M.E., and Shackleton, N.J., 1995. Late Neogene chronology: new perspectives in high-resolution stratigraphy. *Geol. Soc. Am. Bull.,* 107:1272–1287.

Biscaye, P.E., 1964. Distinction between kaolinite and chlorite in Recent sediments by X-ray diffraction. *Am. Mineral.,* 49:1281–1289.

————, 1965. Mineralogy and sedimentation of the Recent deep-sea clay in the Atlantic Ocean and adjacent seas and oceans. *Geol. Soc. Am. Bull.,* 76:803–832.

Boltovskoy, E., 1980. The age of the Drake Passage. *Alcheringa,* 4:289–297.

Broecker, W.S., Bond, G., Klas, M., Bonani, G., and Wolfi, W., 1990. A salt oscillator in the glacial Atlantic? 1. The concept. *Paleoceanography,* 5:469–477.

Cande, S.C., and Kent, D.V., 1995. Revised calibration of the geomagnetic polarity timescale for the Late Cretaceous and Cenozoic. *J. Geophys. Res.,* 100:6093–6095.

Carter, L., Carter, R.M., McCave, I.N., and Gamble, J., 1996. Regional sediment recycling in the abyssal Southwest Pacific Ocean. *Geology,* 24:735–738.

Carter, L., and McCave, I.N., 1994. Development of sediment drifts approaching an active plate margin under the SW Pacific deep western boundary current. *Paleoceanography,* 9:1061–1085.

Carter, L., and Mitchell, J.S., 1987. Late Quaternary sediment pathways through the deep ocean, east of New Zealand. *Paleoceanography,* 2:409–422.

Carter, L., Nelson, C.S., Neil, H.L., and Froggatt, P.C., 1995. Correlation, dispersal, and preservation of the Kawakawa Tephra and other late Quaternary tephra layers in the Southwest Pacific Ocean. *N. Z. J. Geol. Geophys.,* 38:29–46.

Carter, R.M., McCave, I.N., Richter, C., Carter, L., et al., *Proc. ODP, Init. Repts.,* 181: College Station, TX (Ocean Drilling Program).

Flower, B.P., and Kennett, J.P., 1995. Middle Miocene deep water paleoceanography in the southwest Pacific: relations with East Antarctic ice sheet development. *Paleoceanography,* 10:1095–1112.

Fulthorpe, C.S., and Carter, R.M., 1991. Continental-shelf progradation by sediment-drift accretion. *Geol. Soc. Am. Bull.,* 103:300–309.

Fulthorpe, C.S., Carter, R.M., Miller, K.G., and Wilson, J. 1996. The Marshall Paraconformity: a mid-Oligocene record of inception of the Antarctic circumpolar current and coeval glacio-eustatic lowstand. *Mar. Pet. Geol.,* 13:61–77.

Kennett, J.P., Burns, R.E., Andrews, J.E., Churkin, M., Jr., Davies, T.A., Dumitrica, P., Edwards, A.R., Galehouse, J.S., Packham, G.H., and van der Lingen, G.J., 1972. Australian-Antarctic continental drift, paleo-circulation change and Oligocene deep-sea erosion. *Nature,* 239:51–55.

Lawver, L.A., Gahagan, L.M., and Coffin, M.F., 1992. The development of paleoseaways around Antarctica. *In* Kennett, J.P., and Warnke, D.A. (Eds.), *The Antarctic Paleoenvironment: a Perspective on Global Change.* Antarct. Res. Ser., 56:7–30.

Molnar, P., Atwater, T., Mammerickx, J., and Smith, S., 1975. Magnetic anomalies, bathymetry and the tectonic evolution of the South Pacific since the Late Cretaceous. *Geophys. J. R. Astron. Soc.,* 40:383–420.

Moore, D.M., and Reynolds, R.C., 1997. *X-Ray Diffraction and the Identification and Analysis of Clay Minerals* (2nd ed.): Oxford (Oxford Univ. Press).

Nelson, C.S., Froggatt, P.C., and Gosson, G.J., 1986. Nature, chemistry, and origin of late Cenozoic megascopic tephras in Leg 90 cores from the southwestern Pacific. *In* Kennett, J.P., von der Borch, C.C., et al., *Init. Repts. DSDP,* 90: Washington (U.S. Govt. Printing Office), 1161–1171.

Norris, R.J., Carter, R.M., and Turnbull, I.M., 1978. Cainozoic sedimentation in basins adjacent to a major continental transform boundary in southern New Zealand. *J. Geol. Soc. London,* 135:191–205.

Robert, C., Stein, R., and Acquaviva, M., 1986. Cenozoic evolution and significance of clay associations in the New Zealand region of the South Pacific, DSDP Leg 90.

In Kennett, J.P., von der Borch, C.C., et al., *Init. Repts. DSDP,* 90: Washington (U.S. Govt. Printing Office), 1225–1238.

Schmitz, W.J., 1995. On the interbasin-scale thermohaline circulation. *Rev. Geophys.,* 33:151–173.

Shane, P.A.R., and Froggatt, P.C., 1991. Glass chemistry, paleomagnetism, and correlation of middle Pleistocene tuffs in southern North Island, New Zealand, and Western Pacific. *N. Z. J. Geol. Geophys.,* 34:203–211.

Shane, P., Froggatt, P., Black, T., and Westgate, J., 1995. Chronology of Pliocene and Quaternary bioevents and climatic events from fission-track ages on tephra beds, Wairarapa, New Zealand. *Earth Planet. Sci. Lett.,* 130:141–154.

Vella, P., 1962. Age of the younger marine strata at upper Tengawai River (Appendix). *N. Z. J. Geol. Geophys.,* 5:172–174.

Walcott, R.I., 1998. Modes of oblique compression: late Cenozoic tectonics of the South Island of New Zealand. *Rev. Geophys.,* 36:1–26.

Warren, B.A., 1973. Transpacific hydrographic sections at Lats. 43°S and 28°S: the SCORPIO Expedition—II. Deep water. *Deep-Sea Res.,* 20:9–38.

————, 1981. Deep circulation in the world ocean. *In* Warren, B.A., and Wunsch, C. (Eds.), *Evolution of Physical Oceanography:* Cambridge (MIT Press), 6–42.

Winkler, A., Wolf-Welling, T.C.W., Stattegger, K., and Thiede, J., 2001. Clay mineral sedimentation in high northern latitude deep-sea basins since the middle Miocene (ODP Leg 151, NAAG). *Intern. J. Earth Sci.,* 91, 133–148 [Online]. Available from the World Wide Web: <**http://link.springer.de/link/service/journals/00531/contents/01/00199/paper/s005310100199.pdf**>. [Cited 2001-06-08]

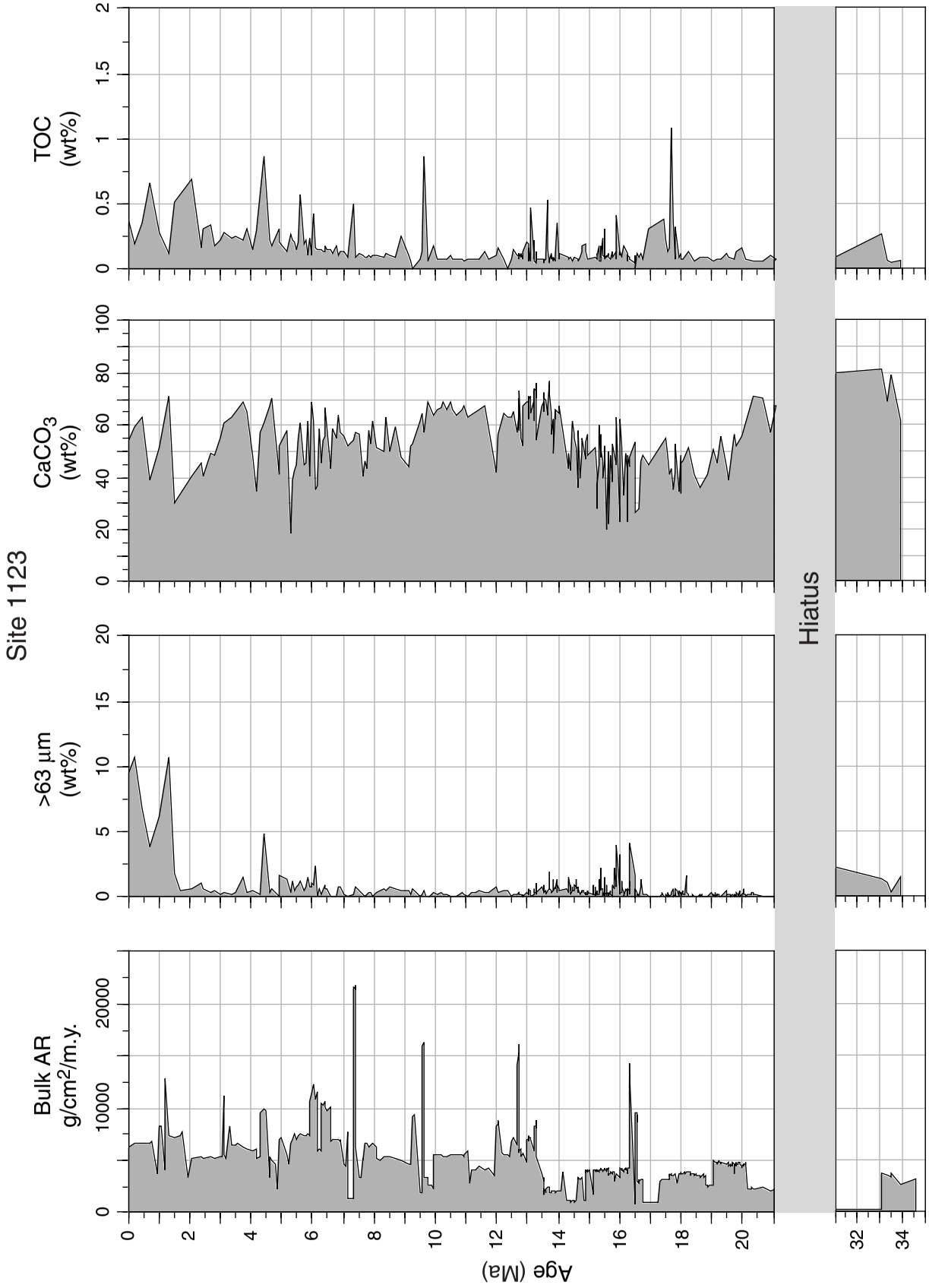

Figure F1. Bulk AR, coarse fraction content, $CaCO_3$ content, and TOC at Site 1123, plotted against age.

Figure F2. Distribution of smectite, illite, chlorite, and kaolinite and the ratio of S/(I+C+S) in the clay fraction at Site 1123, plotted against age.

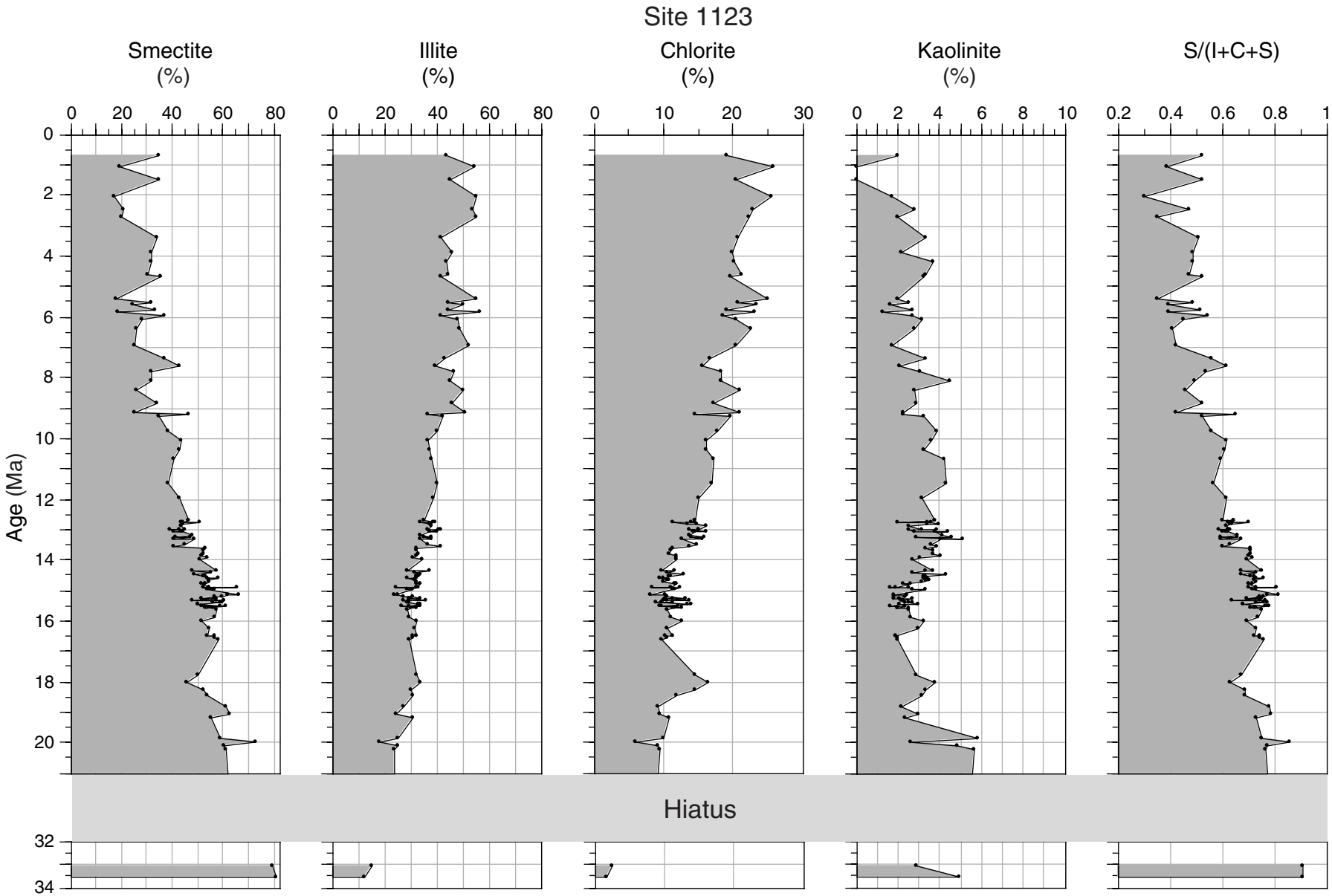

Table T1. Bulk AR, >63 µm, $CaCO_3$, and TOC, Holes 1123B and 1123C. (**See table note.** Continued on next eight pages.)

Core, section, interval (cm)	Depth (mbsf)	Depth (mcd)	Age (Ma)	Bulk AR (g/cm²/m.y.)	>63 µm (wt%)	$CaCO_3$ (wt%)	TOC (wt%)
181-1123B							
1H-1, 12–14	0.12	0.12	0.003	6,358.33	9.6	54.6	0.37
2H-5, 36–38	9.76	9.02	0.216	6,662.50	10.7	59.2	0.20
3H-4, 51–53	17.91	19.63	0.471	6,714.58	6.7	62.8	0.35
4H-4, 89–91	27.79	28.51	0.684	6,730.21	3.9	39.3	0.66
	Datum	32.50	0.780	6,929.17			
	Datum	37.25	0.990	3,813.57			
5H-4, 89–91	37.29	40.19	1.050	8,246.86	6.2	51.6	0.28
	Datum	41.20	1.070	8,299.94			
	Datum	44.35	1.201	4,102.21			
	Datum	45.10	1.211	12,810.00			
6H-5, 70–72	48.10	49.70	1.316	7,404.53	10.7	71.1	0.12
7H-3, 101–103	54.91	58.23	1.510	7,172.86	1.8	30.4	0.51
8H-3, 144–146	64.84	67.94	1.731	7,355.73	0.6		
	Datum	69.65	1.770	7,747.08			
	Datum	73.25	1.950	3,406.51			
9H-2, 100–102	72.40	76.86	2.065	5,225.89	0.6	40.5	0.69
10H-2, 82–84	81.72	86.54	2.374	5,327.71	1.1	45.7	0.17
10H-4, 39–41	84.29	89.11	2.456	5,185.16	0.7	40.8	0.31
11H-2, 129–131	91.69	96.79	2.701	5,382.54	0.4	49.0	0.34
11H-4, 112–114	94.52	99.62	2.792	5,250.95	0.5	48.8	0.19
12H-1, 130–132	99.70	106.64	3.016	5,293.25	0.2	55.0	0.23
	Datum	107.40	3.040	5,323.01			
	Datum	111.85	3.110	11,303.00			
12H-5, 85–87	105.25	112.19	3.121	5,559.20	0.3	60.8	0.28
	Datum	115.30	3.220	5,209.50			
	Datum	120.45	3.330	8,346.51			
13H-6, 38–40	115.78	122.94	3.398	6,529.44	0.2	63.0	0.24
14H-1, 130–132	118.70	127.30	3.517	6,392.19	0.4		0.26
	Datum	129.60	3.580	6,598.98			
14H-6, 99–101	125.89	134.49	3.720	6,279.49	1.5	68.8	0.23
15H-2, 129–131	129.69	139.57	3.866	6,160.07	0.4	65.0	0.32
15H-6, 99–101	135.45	145.33	4.031	6,021.47	0.4	48.5	0.16
	Datum	150.52	4.180	6,157.45			
16H-2, 112–114	139.02	151.04	4.197	5,206.25	0.4	34.5	0.30
	Datum	153.80	4.290	5,358.33			
16H-5, 16–18	142.56	154.58	4.304	9,614.61	0.2	57.1	
17H-3, 125–127	150.15	162.09	4.442	9,957.79	4.9	60.9	0.87
	Datum	164.15	4.480	9,772.58			
	Datum	166.75	4.620	3,455.21			
17H-7, 7–9	154.97	166.91	4.626	5,356.00	0.4	67.2	0.23
18X-2, 5–7	156.95	168.89	4.695	5,047.72	0.7	70.5	0.18
	Datum	171.90	4.800	4,707.96			
	Datum	173.20	4.890	2,319.78			
18X-5, 6–8	161.46	173.40	4.895	6,796.83	0.1	41.0	0.31
19X-1, 38–40	163.08	175.02	4.932	7,089.33	1.7	52.0	0.21
	Datum	177.10	4.980	7,234.50			
19X-6, 8–10	170.38	182.32	5.147	5,619.12	1.3	58.2	0.14
	Datum	184.90	5.230	4,726.80			
20X-2, 88–90	174.70	186.64	5.271	6,720.30	0.3	18.7	0.27
20X-4, 35–37	177.21	189.15	5.330	6,978.45	1.2	39.3	0.23
20X-7, 13–15	181.53	193.47	5.433	7,576.21	0.5	42.7	0.21
21X-1, 140–142	183.30	195.24	5.474	6,999.61	0.8	45.0	0.15
21X-3, 109–111	185.99	197.93	5.538	7,420.69	0.9	55.3	0.21
	Datum	199.96	5.586				
21X-5, 119–121	189.09	201.03	5.611	7,632.00	1.2	61.2	0.58
	Datum	201.55	5.623				
22X-2, 64–66	193.81	205.75	5.723	7,440.39	0.5	44.5	0.19
22X-4, 115–117	197.32	209.26	5.806	7,419.26	0.9	45.5	0.23
22X-6, 91–93	200.08	212.02	5.871	7,655.87	1.5	61.4	0.11
	Datum	213.00	5.894	7,372.79			
23X-1, 71–73	201.91	213.85	5.907	10,676.05	0.8	40.8	0.24
23X-3, 88–90	205.08	217.02	5.957	11,420.74	0.9	69.2	0.11
23X-5, 90–92	208.10	220.04	6.004	11,433.58	1.1	69.1	0.16
24X-1, 40–42	211.20	223.14	6.052	12,229.63	0.9	61.9	0.43
24X-3, 37–39	214.17	226.11	6.098	10,924.81	2.5	35.5	0.17
	Datum	228.60	6.137	11,613.33			
24X-5, 143–145	218.23	230.17	6.184	5,876.02	0.1	36.7	0.15

Table T1 (continued).

Core, section, interval (cm)	Depth (mbsf)	Depth (mcd)	Age (Ma)	Bulk AR (g/cm²/m.y.)	>63 µm (wt%)	$CaCO_3$ (wt%)	TOC (wt%)
24X-7, 8–10	219.88	231.82	6.233	6,159.20	0.7	59.0	0.15
	Datum	233.05	6.269	5,977.16			
25X-1, 134–136	221.74	233.68	6.280	10,244.40	0.3	45.8	0.16
25X-3, 9–11	223.49	235.43	6.310	10,517.37			
25X-5, 9–11	226.49	238.43	6.361	10,282.35		54.6	0.14
25X-7, 10–12	229.50	241.44	6.413	10,609.33	0.9	55.5	0.13
26X-1, 23–25	230.23	242.17	6.425	10,218.12	0.7	66.6	0.18
26X-2, 62–64	232.12	244.06	6.458	9,809.40	0.6	59.2	0.15
	Datum	250.45	6.567	10,060.47			
27X-1, 96–98	240.56	252.50	6.619	6,773.48	0.0	43.7	0.15
27X-3, 56–58	243.16	255.10	6.686	7,066.96	0.1	58.5	0.12
27X-5, 56–58	246.16	258.10	6.763	7,000.43	0.1	54.9	0.19
28X-1, 61–63	249.81	261.75	6.856	6,970.11	0.7	64.0	0.11
28X-3, 46–48	252.66	264.60	6.929	6,931.96	0.8	57.2	0.13
	Datum	264.85	6.935	7,070.87			
28X-5, 52–54	255.72	267.66	7.043	4,665.29	0.2	55.7	0.14
	Datum	268.90	7.091	4,557.55			
	Datum	270.85	7.135	7,804.43			
	Datum	272.00	7.170	5,825.57			
29X-1, 128–130	260.08	272.02	7.172	1,440.12	0.1	52.5	0.10
	Datum	273.40	7.341	1,422.11			
29X-3, 41–43	262.21	274.15	7.347	21,660.88	0.2	54.2	0.51
29X-5, 82–84	265.62	277.56	7.375	21,525.00	0.8	57.6	0.10
	Datum	277.60	7.375	21,840.00			
	Datum	279.60	7.432	6,357.89			
30X-1, 120–122	269.60	281.54	7.537	3,396.92		56.7	0.12
	Datum	282.00	7.562	3,393.23			
30X-3, 102–104	272.42	284.36	7.643	5,228.95	0.2	40.6	0.12
	Datum	284.55	7.650	5,098.55			
30X-5, 119–121	275.59	287.53	7.730	6,716.15	0.1	46.2	0.10
30X-7, 7–9	277.47	289.41	7.781	6,686.48	0.3	43.5	0.10
31X-1, 80–82	278.90	290.84	7.820	6,260.00	0.3	57.7	0.11
31X-3, 51–53	281.61	293.55	7.893	6,460.26	0.3	53.2	0.09
31X-5, 51–53	284.61	296.55	7.974	6,727.27	0.1	61.4	0.10
	Datum	300.20	8.072	6,293.38			
32X-1, 94–96	288.64	300.58	8.085	5,119.22	0.4	51.4	0.11
32X-4, 43–45	292.63	304.57	8.220	5,045.45	0.6		
32X-6, 13–15	295.33	307.27	8.312	5,308.08	0.6	49.9	0.09
33X-1, 45–47	297.75	309.69	8.394	5,458.53	0.5	63.5	0.13
33X-3, 113–115	301.43	313.37	8.518	5,382.56	0.8	49.8	0.11
	Datum	318.70	8.699	5,179.70			
34X-1, 44–46	307.34	319.28	8.719	5,239.20	0.7	59.4	0.09
34X-4, 24–26	311.64	323.58	8.868	5,002.76	0.5	48.1	0.25
	Datum	328.10	9.025				
35X-2, 88–90	318.88	330.82	9.125	4,638.44	0.5	44.3	0.11
35X-4, 43–45	321.43	333.37	9.218	4,687.61	0.3	51.9	0.07
	Datum	333.70	9.230	4,668.49			
35X-6, 26–28	324.26	336.20	9.277	9,167.24	0.7	53.1	0.00
	Datum	337.85	9.308	9,350.80			
36X-2, 99–101	328.39	340.33	9.537	1,988.00	0.1	61.4	0.09
	Datum	340.80	9.580	2,003.18			
36X-4, 34–36	330.74	342.68	9.602	16,025.81	0.2	64.4	0.14
	Datum	346.20	9.642	16,365.48			
36X-6, 99–101	334.39	346.33	9.649	3,418.16	0.5	57.2	0.87
	Datum	348.00	9.740	3,431.02			
37X-1, 92–94	336.42	348.36	9.766	2,590.71	-0.3	69.1	0.07
	Datum	349.95	9.880	2,607.43			
	Datum	350.45	9.920	2,261.25			
37X-3, 92–94	339.42	351.36	9.951	5,490.87	0.4	64.1	0.18
37X-5, 92–94	342.42	354.36	10.053	5,602.22	0.2	66.4	0.08
38X-1, 100–102	346.10	358.04	10.179	5,520.17	0.4	66.7	0.08
38X-3, 93–95	349.03	360.97	10.279	5,321.67	0.2	68.7	0.08
38X-5, 101–103	352.11	364.05	10.384	5,471.83	0.2	65.7	0.08
39X-1, 35–37	355.05	366.99	10.484	5,602.22	0.1	69.0	0.11
39X-3, 38–40	358.08	370.02	10.588	5,625.66	0.1	66.1	0.09
39X-5, 40–42	361.10	373.04	10.691	5,613.94	0.1	63.6	0.08
40X-1, 111–113	365.51	377.45	10.841	5,485.01	0.3	65.7	0.07
40X-3, 111–113	368.51	380.45	10.944	5,411.76	0.2	67.2	0.07
	Datum	380.60	10.949	5,531.90			

Table T1 (continued).

Core, section, interval (cm)	Depth (mbsf)	Depth (mcd)	Age (Ma)	Bulk AR (g/cm²/m.y.)	>63 µm (wt%)	$CaCO_3$ (wt%)	TOC (wt%)
40X-5, 111–113	371.51	383.45	11.037	6,007.23	0.1	62.9	0.08
	Datum	383.95	11.052	5,990.97			
	Datum	384.60	11.099	2,754.89			
41X-1, 98–100	375.08	387.02	11.201	4,059.47	0.4		
41X-3, 98–100	378.08	390.02	11.328	4,110.39	0.3		
41X-5, 95–97	381.05	392.99	11.453	4,433.68	0.5	66.1	0.08
42X-1, 59–61	384.29	396.23	11.590	4,059.47	0.4	67.6	0.14
42X-3, 130–132	388.00	399.94	11.747	4,212.24	0.4		0.08
	Datum	404.40	11.935	3,481.49			
43X-1, 72–74	394.12	406.06	11.970	8,316.43	0.8	41.8	0.10
43X-3, 94–96	397.34	409.28	12.039	8,501.50	0.4	56.8	0.17
	Datum	411.10	12.078	8,787.31			
	Datum	414.75	12.184	5,703.48			
44X-1, 52–54	403.52	415.46	12.207	5,483.99	0.5	64.8	0.08
44X-3, 141–143	407.41	419.35	12.332	5,520.54	0.6	63.3	0.00
	Datum	421.50	12.401	5,398.02			
45X-1, 122–124	413.82	425.76	12.507	6,922.47	0.1	63.2	0.08
45X-2, 25–27	414.35	426.29	12.521	7,154.89	0.2	65.2	0.16
	Datum	432.60	12.678	6,482.84			
	Datum	433.10	12.684				
46X-1, 4–5	422.24	434.18	12.696	14,208.33	0.3	57.1	0.11
46X-1, 46–48	422.66	434.60	12.700	15,345.00	0.3	63.7	0.11
46X-1, 105–107	423.25	435.19	12.707	16,204.37	0.2	70.2	0.12
	Datum	435.30	12.708	16,050.83			
46X-1, 142–144	423.62	435.56	12.716	5,815.22	0.4	67.7	0.10
46X-2, 60–63	424.30	436.24	12.737	5,926.87	0.2	57.9	0.13
46X-2, 106–109	424.76	436.70	12.751	5,933.43	0.2	63.2	0.08
46X-2, 110–114	424.80	436.74	12.752	6,030.30	0.2	62.5	0.09
46X-2, 138–140	425.08	437.02	12.760	5,864.48	0.3	73.2	0.13
	Datum	437.50	12.775	6,156.72			
46X-3, 91–94	426.11	438.05	12.794	5,598.86	0.3	56.3	0.09
46X-3, 135–137	426.55	438.49	12.809	5,318.18	0.2	54.9	0.12
46X-4, 13–15	426.83	438.77	12.818	5,556.02	0.2		
	Datum	438.80	12.819	5,587.05			
46X-4, 42–44	427.12	439.06	12.828	5,640.70	0.1	52.0	0.07
46X-4, 68–70	427.38	439.32	12.836	5,707.85	0.2	57.3	0.10
46X-4, 97–99	427.67	439.61	12.846	5,762.03	0.1		
46X-4, 144–146	428.14	440.08	12.861	5,762.38	0.1	67.5	0.14
	Datum	444.05	12.991	4,911.19			
47X-1, 48–49	432.28	444.22	12.995	6,790.74	0.3	68.9	0.21
47X-1, 94–97	432.74	444.68	13.007	7,000.24	0.3		
47X-1, 120–122	433.00	444.94	13.014	7,051.62	0.2	69.2	0.20
47X-1, 147–149	433.27	445.21	13.020	7,171.78	0.3	71.3	0.07
47X-2, 62–64	433.92	445.86	13.037	7,381.67	0.7	66.1	0.10
47X-2, 132–134	434.62	446.56	13.055	6,869.80	0.3	62.1	
47X-3, 22–23	435.02	446.96	13.065	7,152.42	0.6	69.5	0.17
47X-3, 62–64	435.42	447.36	13.075	7,195.90	0.5		
47X-3, 116–118	435.96	447.90	13.088	7,269.02	0.3	71.2	0.07
47X-3, 141–143	436.21	448.15	13.095	7,229.49	0.1	64.3	0.48
47X-4, 24–27	436.54	448.48	13.103	7,114.86			
	Datum	449.90	13.139	6,481.27			
48X-1, 3–5	441.53	453.47	13.219	5,947.48	0.2	69.9	0.07
48X-1, 44–46	441.94	453.88	13.228	7,649.33	0.7	74.2	0.08
48X-1, 85–87	442.35	454.29	13.237	7,745.61	0.6	66.7	
48X-1, 126–128	442.76	454.70	13.246	7,944.91	0.3	71.7	0.08
48X-2, 2–3	443.02	454.96	13.252	8,106.13		61.7	0.22
48X-2, 14–15	443.14	455.08	13.255	8,370.37	0.3	73.7	0.07
48X-2, 26–28	443.26	455.20	13.257	8,244.97	0.4	74.1	0.05
48X-2, 37–38	443.37	455.31	13.260	8,199.06			
48X-2, 47–48	443.47	455.41	13.262	8,321.10	0.3	72.1	0.07
48X-2, 77–78	443.77	455.71	13.269	8,794.71	0.3	70.6	0.08
48X-2, 88–89	443.88	455.82	13.271	8,737.61		71.0	0.08
48X-2, 96–98	443.96	455.90	13.273	8,468.90	0.3	70.7	0.06
48X-2, 122–123	444.22	456.16	13.279	8,894.36	0.5	72.6	0.07
48X-2, 128–130	444.28	456.22	13.280	8,921.23	0.5	72.2	0.08
48X-2, 149–150	444.49	456.43	13.285	8,721.93		74.0	0.06
48X-3, 7–9	444.57	456.51	13.287	8,831.66	0.6	75.3	0.08
48X-3, 23–24	444.73	456.67	13.290	8,661.47	0.4	76.1	0.07
48X-3, 37–38	444.87	456.81	13.293	8,736.49	1.0	76.0	0.07

Table T1 (continued).

Core, section, interval (cm)	Depth (mbsf)	Depth (mcd)	Age (Ma)	Bulk AR ($g/cm^2/m.y.$)	>63 µm (wt%)	$CaCO_3$ (wt%)	TOC (wt%)
48X-3, 46–48	444.96	456.90	13.295	8,789.11	0.6	73.8	0.13
	Datum	457.20	13.302	8,809.26			
48X-3, 91–92	445.41	457.35	13.307	5,296.63	0.8	58.4	0.08
48X-3, 97–100	445.47	457.41	13.310	5,310.46	0.3	54.1	0.09
49X-1, 2–3	450.82	462.76	13.503	3,784.84	0.8	67.2	0.08
49X-1, 11–12	450.91	462.85	13.506	3,015.99	0.3	69.0	0.08
49X-1, 20–21	451.00	462.94	13.510	3,242.67	0.3	67.1	0.06
	Datum	462.95	13.510	3,440.32			
49X-1, 22–23	451.02	462.96	13.511	1,670.57	0.6	65.1	0.08
49X-1, 31–32	451.11	463.05	13.518	1,993.01	0.3	67.0	0.08
49X-1, 41–42	451.21	463.15	13.526	1,749.91	0.4	68.5	0.08
49X-1, 51–52	451.31	463.25	13.534	1,805.13	0.8	72.5	0.07
49X-1, 61–62	451.41	463.35	13.542	2,215.16	1.0		0.08
49X-1, 83–84	451.63	463.57	13.559	2,347.18	0.3	70.2	0.07
49X-1, 95–96	451.75	463.69	13.568	2,085.67	0.5		
49X-1, 107–108	451.87	463.81	13.578	1,863.52	0.4	69.6	0.09
49X-1, 116–117	451.96	463.90	13.585	1,990.47	0.4		
49X-1, 126–127	452.06	464.00	13.593	2,208.81	0.3		
49X-2, 81–82	453.11	465.05	13.675	2,473.17	0.5	63.6	0.54
49X-2, 92–93	453.22	465.16	13.684	2,427.15	0.5	66.4	0.15
49X-2, 107–108	453.37	465.31	13.696	2,436.04	0.6		
	Datum	465.40	13.703	2,344.64			
49X-2, 128–129	453.58	465.52	13.714	2,024.24	2.0	77.3	0.06
49X-2, 141–142	453.71	465.65	13.727	1,959.15	0.6	71.6	0.08
49X-3, 27–29	454.07	466.01	13.761	1,989.73	0.6	64.3	0.12
49X-3, 35–37	454.15	466.09	13.769	2,035.74	0.4		
49X-3, 50–51	454.30	466.24	13.783	2,071.29	0.3	59.4	0.08
49X-3, 78–79	454.58	466.52	13.810	2,020.05	0.4	56.4	0.11
49X-3, 90–91	454.70	466.64	13.822	2,103.18	0.5	62.8	0.07
49X-3, 107–108	454.87	466.81	13.838	2,033.65	0.5	60.2	0.07
49X-3, 110–111	454.90	466.84	13.841	2,053.51	1.3	58.3	0.08
49X-3, 117–119	454.97	466.91	13.847	2,055.60	0.7	51.4	0.10
49X-3, 130–131	455.10	467.04	13.860	2,112.06	0.6	49.5	0.09
49X-3, 140–142	455.20	467.14	13.869	2,023.19	0.5		
49X-4, 2–4	455.32	467.26	13.881	2,055.18	0.8	65.5	0.06
49X-4, 15–16	455.45	467.39	13.893	2,127.75	0.6	62.4	0.06
49X-4, 30–31	455.60	467.54	13.908	2,125.66	0.6		
49X-4, 47–48	455.77	467.71	13.924	2,003.32	0.7	66.1	0.09
49X-4, 58–59	455.88	467.82	13.934	1,958.36	0.7		
49X-4, 67–68	455.97	467.91	13.943	2,013.78	1.3		
49X-4, 84–87	456.14	468.08	13.959	2,101.61	0.4	65.4	0.36
49X-4, 125–126	456.55	468.49	13.999	2,115.46	0.9		
49X-4, 136–137	456.66	468.60	14.009	2,098.47	0.7	64.6	0.08
49X-4, 147–150	456.77	468.71	14.020	2,076.25	0.5	67.2	0.12
	Datum	469.30	14.076	2,029.90			
	Datum	471.60	14.178	3,988.03			
50X-1, 3–4	460.43	472.37	14.295	1,123.42	0.6		
50X-1, 17–18	460.57	472.51	14.317	1,210.92	0.3		
50X-1, 26–27	460.66	472.60	14.330	1,104.87	0.4	43.1	0.10
	Datum	472.35	14.292				
50X-1, 42–43	460.82	472.76	14.355	1,208.88	1.6	49.3	0.07
50X-1, 56–57	460.96	472.90	14.376	1,209.21	0.7		
50X-1, 69–70	461.09	473.03	14.396	1,172.53	0.5		
	Datum	473.10	14.406				
50X-1, 84–85	461.24	473.18	14.419	1,178.30	0.9	42.5	0.09
50X-1, 90–91	461.30	473.24	14.428	961.06	0.2		
50X-1, 107–108	461.47	473.41	14.454	1,224.83	0.6		
50X-1, 120–121	461.60	473.54	14.473	1,204.51	0.8	61.5	0.07
50X-1, 133–135	461.73	473.67	14.493	1,219.59	0.5		
50X-1, 143–145	461.83	473.77	14.508	1,211.07	0.5		
50X-2, 2–3	461.92	473.86	14.522	1,129.28	0.6		
50X-2, 2–3	461.92	473.86	14.522	1,129.28	0.7	56.8	0.10
50X-2, 17–18	462.07	474.01	14.545	1,079.51	1.0	55.4	0.09
50X-2, 29–30	462.19	474.13	14.563	1,229.09	0.7		
50X-2, 36–39	462.26	474.20	14.574	1,208.45	0.7		
50X-2, 44–46	462.34	474.28	14.586	1,227.45	0.7	51.6	
50X-2, 54–55	462.44	474.38	14.601	1,253.99	1.4		
50X-2, 60–61	462.50	474.44	14.610	1,241.21	0.8		
	Datum	474.45	14.612	1,247.44			

Table T1 (continued).

Core, section, interval (cm)	Depth (mbsf)	Depth (mcd)	Age (Ma)	Bulk AR (g/cm²/m.y.)	>63 µm (wt%)	$CaCO_3$ (wt%)	TOC (wt%)
50X-2, 75–78	462.65	474.59	14.620	3,191.49	0.7	36.2	0.08
50X-2, 79–81	462.69	474.63	14.623	3,206.81	0.8		
50X-2, 89–90	462.79	474.73	14.628	3,267.23	0.8		
50X-2, 117–119	463.07	475.01	14.645	3,297.45	0.6	54.7	
50X-2, 121–122	463.11	475.05	14.647	3,313.62	0.4		
50X-2, 139–140	463.29	475.23	14.658	3,237.45	0.6		
50X-2, 141–143	463.31	475.25	14.659	3,260.00	0.7	58.4	0.07
50X-2, 149–150	463.39	475.33	14.664	3,331.91	0.6		
50X-3, 68–70	464.08	476.02	14.704	3,254.47	0.2	39.5	0.10
50X-4, 7–8	464.97	476.91	14.757	3,331.06	0.5		
50X-4, 38–39	465.28	477.22	14.775	3,428.09	0.3	50.3	0.14
50X-4, 49–50	465.39	477.33	14.781	3,379.15	0.4		
50X-4, 55–56	465.45	477.39	14.785	3,414.47	0.4		
50X-4, 66–67	465.56	477.50	14.791	3,442.55	0.4	55.2	0.19
	Datum	477.65	14.800	3,440.00			
50X-4, 97–98	465.87	477.81	14.826	1,280.16	0.6		
50X-4, 114–115	466.04	477.98	14.853	1,259.06	0.4		
	Datum	478.20	14.888	1,179.62			
50X-5, 5–6	466.45	478.39	14.898	4,077.38	0.3	47.3	0.20
50X-5, 20–21	466.60	478.54	14.905	4,030.21	0.4		
50X-5, 30–31	466.70	478.64	14.910	3,997.43	0.2	53.9	0.14
50X-5, 35–36	466.75	478.69	14.913	4,030.21	0.4		
50X-5, 50–51	466.90	478.84	14.920	3,929.90	0.3		
50X-5, 66–67	467.06	479.00	14.928	3,957.71	0.2		
50X-5, 83–84	467.23	479.17	14.937	4,058.01	0.2		
50X-5, 97–99	467.37	479.31	14.944	3,966.64	0.3	56.7	0.09
50X-5, 114–115	467.54	479.48	14.952	4,042.12	0.3		
50X-5, 128–129	467.68	479.62	14.959	3,946.78	0.4		
50X-5, 140–141	467.80	479.74	14.966	4,014.32	0.2	48.4	0.08
50X-6, 6–7	467.96	479.90	14.974	3,995.45	0.5		
50X-6, 21–22	468.11	480.05	14.981	3,942.81	0.3		
	Datum	481.10	15.034	4,048.00			
51X-1, 9–11	470.09	482.03	15.141	1,748.34	0.2		
	Datum	482.15	15.155	1,789.77			
51X-1, 28–30	470.28	482.22	15.159	4,128.29	1.0		
51X-1, 39–41	470.39	482.33	15.164	4,181.72	0.5		
51X-1, 58–59	470.58	482.52	15.174	4,144.12	0.2		
51X-1, 67–69	470.67	482.61	15.178	4,134.23	0.1		
51X-1, 85–87	470.85	482.79	15.187	4,117.90	0.1		
51X-1, 103–104	471.03	482.97	15.196	4,136.20	0.2	51.7	0.10
51X-1, 116–119	471.16	483.10	15.203	4,005.59	0.1		
51X-1, 136–139	471.36	483.30	15.213	3,958.09	0.3		
51X-2, 12–13	471.62	483.56	15.226	4,146.10	0.8		
51X-2, 25–27	471.75	483.69	15.233	4,058.53	0.4		
51X-2, 40–41	471.90	483.84	15.240	4,074.85	0.2		
51X-2, 53–54	472.03	483.97	15.247	4,092.17	0.3		
51X-2, 66–68	472.16	484.10	15.254	4,051.11	0.3		
51X-2, 83–85	472.33	484.27	15.262	4,027.36	0.2		
51X-2, 99–101	472.49	484.43	15.270	4,037.25	0.4	41.0	0.08
51X-2, 111–112	472.61	484.55	15.276	4,009.55	0.5		
51X-2, 127–129	472.77	484.71	15.284	3,932.36	0.3		
51X-2, 133–135	472.83	484.77	15.287	3,952.65	0.1	28.0	0.12
51X-2, 148–149	472.98	484.92	15.295	4,037.25	0.3	37.4	0.12
51X-3, 10–11	473.10	485.04	15.301	3,950.17	0.2		
51X-3, 27–28	473.27	485.21	15.310	4,074.85	0.3		
51X-3, 43–44	473.43	485.37	15.318	4,096.62	0.2	45.1	0.19
51X-3, 60–62	473.60	485.54	15.326	4,148.08	1.5		
51X-3, 74–75	473.74	485.68	15.333	4,030.33	0.5		
51X-3, 88–90	473.88	485.82	15.340	4,051.11	1.4		
51X-3, 103–104	474.03	485.97	15.348	4,084.75	0.8	60.1	0.07
51X-3, 118–120	474.18	486.12	15.356	4,056.05	0.4		
51X-3, 137–139	474.37	486.31	15.365	4,025.87	1.6		
51X-4, 8–9	474.58	486.52	15.376	4,219.32	0.8		
51X-4, 11–13	474.61	486.55	15.377	4,221.30	1.9	47.8	0.06
51X-4, 24–26	474.74	486.68	15.384	4,118.39	2.0		
51X-4, 37–39	474.87	486.81	15.390	4,089.20	1.8	56.5	0.18
51X-4, 53–55	475.03	486.97	15.399	4,100.58	0.5		
51X-4, 66–68	475.16	487.10	15.405	4,077.82	2.2		
51X-4, 82–83	475.32	487.26	15.413	4,124.33	1.3	50.8	0.10

Table T1 (continued).

Core, section, interval (cm)	Depth (mbsf)	Depth (mcd)	Age (Ma)	Bulk AR (g/cm²/m.y.)	>63 µm (wt%)	$CaCO_3$ (wt%)	TOC (wt%)
51X-4, 98–99	475.48	487.42	15.421	4,144.12	0.7		
51X-4, 115–117	475.65	487.59	15.430	4,165.89	0.6		
51X-4, 131–132	475.81	487.75	15.438	4,009.55	0.5	46.3	0.24
51X-4, 147–148	475.97	487.91	15.446	4,079.60	0.3		
51X-5, 15–16	476.15	488.09	15.455	4,118.39	0.4		
51X-5, 27–29	476.27	488.21	15.461	4,098.60	0.2	39.4	0.11
51X-5, 46–47	476.46	488.40	15.471	4,058.03	0.1		
51X-5, 68–70	476.68	488.62	15.482	4,116.41	0.3		
51X-5, 84–86	476.84	488.78	15.490	4,144.12	0.0	46.3	
51X-5, 96–98	476.96	488.90	15.496	4,138.18	1.6		
51X-5, 112–114	477.12	489.06	15.504	4,185.68			
51X-5, 127–129	477.27	489.21	15.512	4,169.85	0.9	52.3	0.09
51X-5, 145–147	477.45	489.39	15.521	4,160.67	1.1		
51X-6, 15–16	477.66	489.60	15.531	4,213.39	0.2		
51X-6, 27–29	477.78	489.72	15.538	4,064.96	0.2	50.2	0.31
51X-6, 42–44	477.92	489.87	15.545	4,096.62	0.3	51.3	0.08
51X-6, 50–52	478.01	489.95	15.549	4,118.39	0.3		
51X-6, 64–65	478.15	490.09	15.556	4,082.77	0.2		
51X-6, 76–78	478.27	490.21	15.562	3,914.55	0.1	20.0	0.12
51X-6, 93–95	478.44	490.38	15.571	4,088.71	0.1		
51X-6, 115–116	478.66	490.60	15.582	4,136.20	0.1		
51X-6, 127–128	478.78	490.72	15.588	4,203.49	0.1	22.1	0.10
51X-6, 143–145	478.94	490.88	15.596	4,062.98	0.9		
51X-7, 9–10	479.10	491.04	15.604	4,188.15	0.3		
51X-7, 23–25	479.24	491.18	15.611	4,215.37	0.2	50.2	0.13
51X-7, 42–44	479.43	491.37	15.621	3,635.51	0.4		
52X-1, 19–21	479.49	491.43	15.624	3,746.33	0.1	22.6	0.09
181-1123C-							
18X-1, 0–2	484.00	492.70	15.688	3,788.68	0.6		
18X-1, 50–52	484.50	493.20	15.713	3,910.59	0.3	48.5	0.08
18X-1, 99–101	484.99	493.69	15.738	3,787.89	0.1		
18X-1, 148–150	485.48	494.18	15.763	3,815.60	0.2	38.0	0.13
18X-2, 50–52	486.00	494.70	15.789	3,897.73	0.6		
181-1123B-							
52X-3, 50–52	482.80	494.74	15.791	3,856.17	1.0	53.1	0.10
181-1123C-							
18X-2, 100–102	486.50	495.20	15.814	3,882.89	0.7		
18X-2, 140–150	486.90	495.60	15.835	3,022.61	2.3		
18X-3, 49–51	487.49	496.19	15.864	3,784.43	0.9	44.6	0.13
18X-3, 83–85	487.83	496.53	15.882	3,726.54	1.0	51.1	0.08
18X-3, 100–102	488.00	496.70	15.890	3,708.73	1.8		
18X-3, 148–150	488.48	497.18	15.914	3,811.64	4.0	63.1	0.41
19X-1, 50–52	489.00	498.56	15.984	3,417.81	0.4		
181-1123B-							
52X-5, 146–148	486.76	498.70	15.991	3,410.69	0.2	23.3	0.12
181-1123C-							
19X-1, 79–81	489.29	498.85	15.999	3,597.90	0.3	27.9	0.12
19X-1, 98–100	489.48	499.04	16.008	3,778.00	3.2	62.3	0.14
	Datum	499.15	16.014	3,744.85			
19X-1, 148–150	489.98	499.54	16.032	4,243.91	0.3		
19X-2, 50–52	490.50	500.06	16.057	4,030.65	0.3	51.6	0.10
19X-2, 100–102	491.00	500.56	16.080	4,252.44	1.3		
19X-2, 148–150	491.48	501.04	16.103	4,191.02	0.8	49.4	0.12
19X-3, 48–50	491.98	501.54	16.126	3,945.34	0.3		
19X-3, 98–100	492.48	502.04	16.150	4,062.63	0.1	33.3	0.18
19X-3, 148–150	492.98	502.54	16.173	4,254.57	0.6		
19X-4, 49–51	493.49	503.05	16.197	4,138.88	0.7	49.5	
19X-4, 99–101	493.99	503.55	16.220	4,203.39	0.5		
19X-4, 134–136	494.34	503.90	16.237	3,980.43	0.7	41.5	0.13
19X-5, 16–18	494.66	504.22	16.252	3,796.06	0.1	23.2	0.06
19X-5, 48–50	494.98	504.54	16.267	4,297.22	0.4		
19X-5, 100–102	495.50	505.06	16.291	4,258.84	0.5	48.3	0.10
	Datum	505.10	16.293	4,292.96			
19X-5, 148–150	495.98	505.54	16.299	13,617.88	0.6		
19X-6, 50–52	496.50	506.06	16.307	13,958.82	0.3	43.8	0.10
19X-6, 98–100	496.98	506.54	16.313	14,110.59	1.2		
19X-6, 148–150	497.48	507.04	16.320	14,090.82	0.8	48.1	0.08

Table T1 (continued).

Core, section, interval (cm)	Depth (mbsf)	Depth (mcd)	Age (Ma)	Bulk AR ($g/cm^2/m.y.$)	>63 µm (wt%)	$CaCO_3$ (wt%)	TOC (wt%)
19X-7, 25–27	497.75	507.31	16.324	14,315.29	4.2		
	Datum	507.50	16.327	13,374.90			
20X-1, 50–52	498.60	508.16	16.479	849.78	1.7	53.4	0.05
	Datum	508.20	16.488	848.04			
20X-1, 102–104	499.12	508.68	16.498	8,585.88	0.3		
20X-1, 147–149	499.57	509.13	16.508	8,928.94	0.1	33.0	0.11
20X-2, 47–49	500.07	509.63	16.518	8,795.29	0.2		
20X-2, 54–56	500.14	509.70	16.520	8,840.00	0.0	26.8	0.00
20X-2, 99–100	500.59	510.15	16.529	9,543.53	0.7		
20X-2, 148–150	501.08	510.64	16.540	9,493.65	0.3		
20X-3, 48–50	501.58	511.14	16.550	8,705.88	0.1	27.6	0.12
	Datum	511.40	16.556	9,329.41			
20X-3, 95–97	502.05	511.61	16.570	2,931.88	0.2		
20X-3, 147–149	502.57	512.13	16.604	2,918.27	0.2	28.2	0.10
20X-4, 51–53	503.11	512.67	16.639	3,116.94	0.2		
20X-4, 59–60	503.19	512.75	16.644	2,973.18	0.1	28.0	0.10
20X-4, 97–99	503.57	513.13	16.669	3,144.09	0.8	46.2	0.12
20X-4, 148–150	504.08	513.64	16.702	3,161.29	1.4		
	Datum	514.00	16.726	3,251.53			
20X-5, 51–53	504.61	514.17	16.759	1,081.55	0.2	48.3	0.08
20X-5, 100–102	505.10	514.66	16.854	1,081.55	0.2		
20X-5, 148–150	505.58	515.14	16.946	1,063.03	0.1	45.0	0.32
20X-6, 50–52	506.10	515.66	17.047	1,046.64	0.1		
	Datum	516.85	17.277	978.73			
21X-1, 48–50	508.18	517.74	17.334	3,030.40	0.1		
21X-1, 98–100	508.68	518.24	17.366	3,143.79	0.1		
21X-1, 148–150	509.18	518.74	17.399	3,149.69	0.3		
21X-2, 47–49	509.67	519.23	17.430	3,106.51	0.1		
21X-2, 99–101	510.19	519.75	17.464	3,131.36	0.1		0.38
21X-2, 148–150	510.68	520.24	17.495	3,167.40	0.1		
21X-3, 50–52	511.20	520.76	17.529	3,103.40	0.2	55.5	0.23
21X-3, 74–76	511.44	521.00	17.544	3,157.77	0.0	48.7	0.13
21X-3, 100–102	511.70	521.26	17.561	3,122.04	0.1		
21X-3, 148–150	512.18	521.74	17.592	3,139.44	0.3		
	Datum	522.10	17.615	3,119.71			
21X-4, 48–50	512.68	522.24	17.623	3,679.28	0.1		
21X-4, 99–101	513.19	522.75	17.651	3,553.15	0.1	41.3	0.17
21X-4, 148–150	513.68	523.24	17.678	3,668.11	0.2		
21X-5, 50–52	514.20	523.76	17.707	3,621.62	0.3	43.2	1.09
21X-5, 100–102	514.70	524.26	17.735	3,619.82	0.7		
21X-5, 148–150	515.18	524.74	17.762	3,583.78	0.1	35.3	0.36
21X-6, 49–51	515.69	525.25	17.790	3,664.41	0.2		
21X-6, 72–73	515.92	525.48	17.803	3,650.45	0.1	41.8	0.08
21X-6, 100–102	516.20	525.76	17.818	3,684.68	0.6	52.6	0.33
21X-6, 147–149	516.67	526.23	17.844	2,883.96	0.6		
22X-1, 50–52	517.90	527.46	17.912	3,774.77	0.1	34.9	0.09
22X-1, 99–101	518.39	527.95	17.940	3,814.41	0.4		
22X-1, 148–150	518.88	528.44	17.967	3,687.57	0.2	48.8	0.12
22X-2, 48–50	519.38	528.94	17.995	3,864.86	0.4		
22X-2, 69–72	519.59	529.15	18.006	3,675.23	0.0	34.3	0.10
22X-2, 100–102	519.90	529.46	18.023	3,751.35	0.1	45.8	0.08
22X-2, 149–150	520.39	529.95	18.051	3,763.96	0.5		
22X-3, 49–51	520.89	530.45	18.078	3,775.68	0.2	46.4	0.08
22X-3, 99–101	521.39	530.95	18.106	3,850.45	0.2		
22X-3, 148–150	521.88	531.44	18.133	3,814.05	0.2		
22X-4, 50–52	522.40	531.96	18.162	3,914.41	1.6		
22X-4, 98–100	522.88	532.44	18.189	3,876.58	0.4		
22X-5, 49–51	523.89	533.45	18.245	3,862.61	0.3		
22X-5, 74–77	524.14	533.70	18.259	3,928.83	0.1	51.6	0.14
22X-5, 97–99	524.37	533.93	18.272	3,834.68	0.1		
	Datum	534.10	18.281	3,912.61			
22X-5, 148–150	524.88	534.44	18.301	3,634.36	0.1		
22X-6, 49–51	525.39	534.95	18.330	3,700.58	0.1		
22X-6, 99–101	525.89	535.45	18.359	3,771.96	0.1		
22X-6, 148–150	526.38	535.94	18.388	3,777.81	0.2		
23X-1, 49–51	527.49	537.05	18.453	3,664.46	0.1		
23X-1, 59–61	527.59	537.15	18.458	3,612.00	0.0	40.9	0.07
23X-1, 100–102	528.00	537.56	18.482	3,660.16	0.1		
23X-1, 148–150	528.48	538.04	18.510	3,594.46	0.1		

Table T1 (continued).

Core, section, interval (cm)	Depth (mbsf)	Depth (mcd)	Age (Ma)	Bulk AR (g/cm²/m.y.)	>63 µm (wt%)	$CaCO_3$ (wt%)	TOC (wt%)
23X-2, 46–48	528.96	538.52	18.538	3,619.74	0.1		
23X-2, 100–102	529.50	539.06	18.569	3,541.48	0.1		
23X-2, 148–150	529.98	539.54	18.597	3,535.29	0.3		
23X-3, 48–50	530.48	540.04	18.626	3,574.16	0.1	36.4	0.09
23X-3, 51–53	530.51	540.07	18.628	3,381.52	0.1		
23X-3, 100–102	531.00	540.56	18.657	3,500.20	0.2		
23X-3, 148–150	531.48	541.04	18.684	3,582.76	0.1		
23X-4, 50–52	532.00	541.56	18.715	3,729.82	0.1		
23X-4, 101–103	532.51	542.07	18.744	3,438.71	0.1		
23X-4, 148–150	532.98	542.54	18.772	3,570.38	0.1		
	Datum	542.70	18.781	3,562.98			
23X-5, 48–50	533.48	543.04	18.809	2,616.52	0.1		
23X-5, 94–96	533.94	543.50	18.846	2,618.99	0.0	41.4	0.09
23X-5, 100–102	534.00	543.56	18.851	2,614.04	0.1		
23X-5, 148–150	534.48	544.04	18.889	2,494.90	0.1		
23X-6, 50–52	535.00	544.56	18.931	2,614.04	0.2		
23X-6, 97–99	535.47	545.03	18.970	2,667.19	0.4		
23X-6, 148–150	535.98	545.54	19.011	2,600.20	0.3		
	Datum	546.00	19.048	2,583.15			
24X-1, 25–27	536.85	546.41	19.065	4,816.08	0.0	50.5	0.07
24X-1, 49–51	537.09	546.65	19.075	4,946.00	0.2		
24X-1, 98–100	537.58	547.14	19.096	4,816.08	0.1		
24X-1, 148–150	538.08	547.64	19.117	4,875.64	0.4		
24X-2, 50–52	538.60	548.16	19.139	4,780.48	0.1		
24X-2, 97–99	539.07	548.63	19.159	4,762.09	0.2		
24X-2, 148–150	539.58	549.14	19.180	4,741.80	0.2		
24X-3, 27–29	539.87	549.43	19.193	4,762.69	0.0	45.3	0.09
24X-3, 49–51	540.09	549.65	19.202	4,720.57	0.2		
24X-3, 98–100	540.58	550.14	19.222	4,981.01	0.2		
24X-3, 148–150	541.08	550.64	19.244	4,749.87	0.1		
24X-4, 50–52	541.60	551.16	19.265	4,787.60	0.1		
24X-4, 100–102	542.10	551.66	19.287	4,760.31	0.1		
24X-4, 148–150	542.58	552.14	19.307	4,710.95	0.1		
24X-5, 8–10	542.68	552.24	19.311	4,812.52	0.1	55.5	0.08
25X-6, 19–20	553.89	563.45	19.463	4,617.93	0.4	44.4	0.13
25X-6, 49–51	554.19	563.75	19.476	4,615.56	0.1		
25X-6, 101–103	554.71	564.27	19.498	4,695.65	0.1		
25X-6, 143–145	555.13	564.69	19.515	4,869.47	0.3		
26X-1, 49–51	556.19	565.75	19.560	4,703.95	0.2		
26X-1, 66–68	556.36	565.92	19.567	4,506.40	0.2	38.9	0.10
26X-1, 98–100	556.68	566.24	19.581	4,608.44	0.2		
26X-1, 148–150	557.18	566.74	19.602	4,542.47	0.2		
26X-2, 50–52	557.70	567.26	19.624	4,508.77	0.1		
26X-2, 100–102	558.20	567.76	19.645	4,710.48	0.2		
26X-2, 148–150	558.68	568.24	19.665	4,537.25	0.2		
26X-3, 48–50	559.18	568.74	19.686	4,779.30	0.2		
26X-3, 92–94	559.62	569.18	19.705	4,722.35	0.1	56.9	0.09
26X-3, 98–100	559.68	569.24	19.707	4,648.78	0.1		
26X-3, 148–150	560.18	569.74	19.728	3,704.31	0.1		
26X-4, 49–51	560.69	570.25	19.750	4,555.64	0.2		
26X-4, 104–106	561.24	570.80	19.773	4,750.82	0.1		
26X-4, 148–150	561.68	571.24	19.791	4,551.96	0.1		
26X-5, 48–50	562.18	571.74	19.812	4,679.63	0.1		
26X-5, 62–64	562.32	571.88	19.818	4,645.22	0.3	52.3	0.13
26X-5, 98–100	562.68	572.24	19.833	4,736.58	0.2		
26X-5, 148–150	563.18	572.74	19.855	4,739.43	0.1		
26X-6, 49–51	563.69	573.25	19.876	4,863.54	0.1		
26X-6, 99–101	564.19	573.75	19.897	4,786.42	0.5		
26X-6, 148–150	564.68	574.24	19.918	4,700.99	0.1		
27X-1, 49–51	565.89	575.45	19.969	4,476.14	0.1		
27X-1, 78–80	566.18	575.74	19.981	4,378.25	0.0	56.0	0.17
27X-1, 100–102	566.40	575.96	19.990	4,449.45	0.2		
27X-1, 148–150	566.88	576.44	20.010	4,650.20	0.4		
27X-2, 48–50	567.38	576.94	20.032	4,489.79	0.6		
27X-2, 98–100	567.88	577.44	20.053	4,609.63	0.3		
27X-2, 148–150	568.38	577.94	20.074	4,688.17	0.2		
27X-3, 50–52	568.90	578.46	20.096	4,756.75	0.2		
27X-3, 103–105	569.43	578.99	20.118	4,610.81	0.1		
27X-3, 132–134	569.72	579.28	20.130	4,565.72	0.0	60.8	0.07

Table T1 (continued).

Core, section, interval (cm)	Depth (mbsf)	Depth (mcd)	Age (Ma)	Bulk AR ($g/cm^2/m.y.$)	>63 µm (wt%)	$CaCO_3$ (wt%)	TOC (wt%)
	Datum	579.30	20.131				
27X-3, 148–150	569.88	579.44	20.143	2,261.88	0.2		
27X-4, 50–52	570.40	579.96	20.187	2,264.72	0.2		
27X-4, 100–102	570.90	580.46	20.229	2,301.44	0.2		
27X-4, 148–150	571.38	580.94	20.269	2,345.03	0.2		
27X-5, 47–49	571.87	581.43	20.311	2,509.91	0.3		
27X-5, 65–67	572.05	581.61	20.326	2,273.31	0.4	71.3	0.06
27X-5, 98–100	572.38	581.94	20.354	2,246.96	0.3		
27X-5, 148–150	572.88	582.44	20.396	2,350.95	0.3		
28X-1, 94–96	576.04	585.60	20.663	2,381.99	0.1	70.8	0.07
28X-3, 85–87	578.95	588.51	20.909	2,124.07	0.1	57.3	0.11
28X-5, 40–41	581.50	591.06	21.124	2,353.56	0.0	67.6	0.09
29X-1, 45–47	585.15	594.71	21.432	2,114.30	0.1	64.9	0.15
	BioDatum	596.70	21.600	2,329.28			
	BioDatum	597.00	30.000				
29X-3, 88–90	588.58	598.14	31.025	227.93	2.3	80.3	0.10
	Datum	600.40	33.058	245.77			
29X-5, 50–52	591.20	600.76	33.078	3,776.41	1.5	81.7	0.26
30X-2, 7–9	595.87	605.43	33.343	3,630.72	1.1	69.1	0.06
30X-4, 32–34	599.12	608.68	33.527	3,387.02	0.4	78.9	0.05
	Datum	609.00	33.545	3,740.21			
31X-1, 121–123	605.11	614.67	33.930	2,674.92	1.5	61.5	0.06
	Datum	625.35	34.655	3,178.68			

Note: AR = accumulation rate, TOC = total organic carbon.

Table T2. Smectite, illite, kaolinite, chlorite, and the ratio between S/(I+C+S), Holes 1123B and 1123C. (Continued on next page.)

Core, section, interval (cm)	Depth (mcd)	Age (Ma)	Smectite (%)	Illite (%)	Kaolinite (%)	Chlorite (%)	S/(I+C+S)
181-1123B-							
4H-4, 89–91	28.51	0.684	34	44	2	19	0.52
5H-4, 89–91	40.19	1.050	20	55	0	26	0.39
7H-3, 101–103	58.23	1.510	35	45	0	20	0.52
9H-2, 100–102	76.86	2.065	18	55	2	26	0.30
10H-4, 39–41	89.11	2.456	21	54	3	23	0.47
11H-2, 129–131	96.79	2.701	20	55	2	22	0.35
13H-6, 38–40	122.94	3.398	34	42	3	21	0.51
15H-2, 129–131	139.57	3.866	32	46	2	20	0.49
16H-2, 112–114	151.04	4.197	32	44	4	20	0.49
17H-7, 7–9	166.91	4.626	31	45	3	21	0.47
18X-2, 5–7	168.89	4.695	36	41	3	20	0.53
20X-7, 13–15	193.47	5.433	18	55	2	25	0.35
21X-3, 109–111	197.93	5.538	32	45	3	21	0.49
21X-5, 119–121	201.03	5.611	24	51	2	23	0.40
22X-4, 115–117	209.26	5.806	34	45	3	19	0.51
22X-6, 91–93	212.02	5.871	19	57	1	23	0.40
23X-3, 88–90	217.02	5.957	37	42	3	19	0.55
24X-3, 37–39	226.11	6.098	29	48	3	20	0.46
25X-7, 10–12	241.44	6.413	26	49	3	23	0.41
28X-3, 46–48	264.60	6.929	25	53	2	20	0.42
29X-3, 41–43	274.15	7.347	37	43	3	17	0.56
30X-3, 102–104	284.36	7.643	43	39	2	16	0.62
31X-1, 80–82	290.84	7.820	32	47	3	18	0.54
32X-1, 94–96	300.58	8.085	32	45	5	18	0.50
33X-1, 45–47	309.69	8.394	26	50	3	21	0.46
34X-4, 24–26	323.58	8.868	34	46	3	17	0.53
35X-2, 88–90	330.82	9.125	25	51	2	21	0.42
35X-4, 43–45	333.37	9.218	47	37	2	15	0.65
35X-6, 26–28	336.20	9.277	35	42	3	20	0.52
37X-1, 92–94	348.36	9.766	38	40	4	18	0.56
37X-5, 92–94	354.36	10.053	44	36	4	16	0.62
38X-5, 101–103	364.05	10.384	43	37	3	16	0.61
39X-5, 40–42	373.04	10.691	40	38	4	17	0.59
41X-5, 95–97	392.99	11.453	38	40	4	17	0.57
43X-1, 72–74	406.06	11.970	43	39	3	15	0.62
46X-1, 4–5	434.18	12.696	46	35	4	15	0.60
46X-1, 105–107	435.19	12.707	46	35	4	15	0.65
46X-2, 60–63	436.24	12.737	44	40	2	14	0.64
46X-2, 110–114	436.74	12.752	43	39	3	15	0.62
46X-2, 138–140	437.02	12.760	51	34	4	11	0.70
46X-4, 42–44	439.06	12.828	44	38	4	13	0.64
46X-4, 68–70	439.32	12.836	44	37	3	15	0.63
46X-4, 144–146	440.08	12.861	43	38	3	16	0.62
47X-1, 94–97	444.68	13.007	45	37	3	15	0.63
47X-1, 120–122	444.94	13.014	39	42	4	15	0.59
47X-2, 62–64	445.86	13.037	43	41	3	14	0.63
47X-3, 22–23	446.96	13.065	44	37	3	16	0.62
47X-3, 116–118	447.90	13.088	41	40	4	14	0.60
47X-3, 141–143	448.15	13.095	44	37	4	14	0.63
48X-1, 3–5	453.47	13.219	48	34	4	14	0.66
48X-1, 44–46	453.88	13.228	41	38	5	16	0.60
48X-2, 96–98	455.90	13.273	47	36	3	14	0.66
48X-3, 7–9	456.51	13.287	41	38	5	16	0.59
48X-3, 97–100	457.41	13.310	49	34	4	13	0.68
49X-1, 31–32	463.05	13.518	45	37	4	15	0.64
49X-1, 83–84	463.57	13.559	40	42	4	14	0.61
49X-1, 126–127	464.00	13.593	53	32	3	11	0.71
49X-2, 128–129	465.52	13.714	53	32	4	11	0.71
49X-3, 50–51	466.24	13.783	52	33	4	11	0.71
49X-3, 110–111	466.84	13.841	52	32	4	12	0.70
49X-4, 67–68	467.91	13.943	54	31	3	12	0.72
49X-4, 147–150	468.71	14.020	51	34	3	12	0.70
50X-1, 26–27	472.60	14.330	57	29	4	10	0.75
50X-1, 42–43	472.76	14.355	48	37	3	12	0.68
50X-1, 84–85	473.18	14.419	55	32	3	11	0.73
50X-1, 120–121	473.54	14.473	49	34	4	13	0.67
50X-2, 2–3	473.86	14.522	52	33	3	11	0.71

Table T2 (continued).

Core, section, interval (cm)	Depth (mcd)	Age (Ma)	Smectite (%)	Illite (%)	Kaolinite (%)	Chlorite (%)	S/(I+C+S)
50X-2, 17–18	474.01	14.545	53	33	3	11	0.72
50X-2, 44–46	474.28	14.586	54	32	3	10	0.73
50X-2, 75–78	474.59	14.620	59	29	3	10	0.76
50X-2, 117–119	475.01	14.645	54	32	3	11	0.73
50X-2, 141–143	475.25	14.659	54	32	4	11	0.73
50X-3, 68–70	476.02	14.704	55	32	3	10	0.74
50X-4, 38–39	477.22	14.775	53	33	2	12	0.72
50X-4, 66–67	477.50	14.791	52	34	3	12	0.71
50X-5, 5–6	478.39	14.898	55	32	2	11	0.73
50X-5, 30–31	478.64	14.910	65	24	2	9	0.81
50X-5, 50–51	478.84	14.920	52	33	3	12	0.70
50X-5, 97–99	479.31	14.944	56	29	3	12	0.73
50X-5, 140–141	479.74	14.966	54	31	3	11	0.72
51X-1, 9–11	482.03	15.141	66	24	2	8	0.82
51X-1, 58–59	482.52	15.174	62	26	2	10	0.78
51X-1, 103–104	482.97	15.196	60	28	2	11	0.76
51X-2, 12–13	483.56	15.226	57	31	2	11	0.75
51X-2, 53–54	483.97	15.247	51	34	2	13	0.69
51X-2, 99–101	484.43	15.270	56	30	2	11	0.74
51X-2, 133–135	484.77	15.287	58	29	3	10	0.75
51X-3, 43–44	485.37	15.318	48	36	2	14	0.64
51X-3, 88–90	485.82	15.340	57	30	2	11	0.75
51X-3, 137–139	486.31	15.365	60	27	2	10	0.77
51X-4, 11–13	486.55	15.377	60	29	2	9	0.77
51X-4, 37–39	486.81	15.390	56	30	3	11	0.74
51X-4, 82–83	487.26	15.413	59	29	3	10	0.76
51X-4, 131–132	487.75	15.438	50	33	3	14	0.68
51X-5, 27–29	488.21	15.461	50	34	2	14	0.68
51X-5, 84–86	488.78	15.490	59	30	2	9	0.77
51X-5, 127–129	489.21	15.512	52	34	2	12	0.78
51X-6, 27–29	489.72	15.538	61	27	2	10	0.78
51X-6, 76–78	490.21	15.562	53	32	2	13	0.71
51X-7, 23–25	491.18	15.611	56	30	3	11	0.73
52X-1, 19–21	491.43	15.624	58	29	3	11	0.75
181-1123C-							
18X-3, 83–85	496.53	15.882	57	30	3	11	0.74
181-1123B-							
52X-5, 146–148	498.70	15.991	51	33	3	13	0.69
181-1123C-							
19X-5, 16–18	504.22	16.252	55	31	3	11	0.73
20X-1, 50–52	508.16	16.479	54	33	2	11	0.73
20X-2, 99–100	510.15	16.529	57	31	2	10	0.75
20X-3, 147–149	512.13	16.604	58	30	2	10	0.76
21X-6, 72–73	525.48	17.803	50	33	3	15	0.67
22X-2, 69–72	529.15	18.006	46	34	4	16	0.63
22X-5, 74–77	533.70	18.259	52	30	3	15	0.69
23X-1, 59–61	537.15	18.458	54	31	3	12	0.69
23X-5, 94–96	543.50	18.846	61	28	2	9	0.78
24X-1, 25–27	546.41	19.065	63	25	3	9	0.79
24X-3, 27–29	549.43	19.193	55	31	2	11	0.73
25X-6, 19–20	563.45	19.463	59	25	6	10	0.75
26X-1, 66–68	565.92	19.567	73	18	3	6	0.86
26X-3, 92–94	569.18	19.705	61	25	5	9	0.77
26X-5, 62–64	571.88	19.818	61	24	6	9	0.77
29X-5, 50–52	600.76	33.078	79	15	3	3	0.91
30X-4, 32–34	608.68	33.527	81	12	5	2	0.91